Research in Astron. Astrophys. **2013** Vol. **13** No. **5**, 526–536
http://www.raa-journal.org *http://www.iop.org/journals/raa*

Research in Astronomy and Astrophysics

The contracting and unshearing motion of flare loops in the X 7.1 flare on 2005 January 20 during its rising phase *

Tuan-Hui Zhou[1,4,5], Jun-Feng Wang[2], Dong Li[1,3,5], Qi-Wu Song[1,4,5], Victor Melnikov[1] and Hai-Sheng Ji[1,5]

[1] Key Laboratory for Dark Matter and Space Science, Purple Mountain Observatory, Chinese Academy of Sciences, Nanjing 210008, China
[2] School of Physics Optoelectronic Engineering, Nanjing University of Information Science and Technology, Nanjing 210044, China
[3] Graduate University of Chinese Academy of Sciences, Beijing 100049, China
[4] Key Laboratory of Solar Activity, National Astronomical Observatories, Chinese Academy of Sciences, Beijing 100012, China
[5] Purple Mountain Observatory, Chinese Academy of Sciences, Nanjing 210008, China; *thzhou@pmo.ac.cn*

Received 2012 October 21; accepted 2012 December 30

Abstract With the aim of studying the relationship between the relative motions of the loop-top (LT) source and footpoints (FPs) during the rising phase of solar flares, we give a detailed analysis of the X7.1 class flare that occurred on 2005 January 20. The flare was clearly observed by *RHESSI*, showing a distinct X-ray flaring loop with a bright LT source and two well-defined hard X-ray (HXR) FPs. In particular, we correct the projection effect for the positions of the FPs and magnetic polarity inversion line. We find that: (1) The LT source showed an obvious U-shaped trajectory. The source of the higher energy LT shows a faster downward/upward speed. (2) The evolution of FPs was temporally correlated with that of the LT source. The converging/separating motion of FPs corresponds to the downward/upward motion of the LT source. (3) The initial flare shear of this event is found to be nearly 50 degrees, and it has a fluctuating decrease throughout the contraction phase as well as the expansion phase. (4) Four peaks of the time profile of the unshearing rate are found to be temporally correlated with peaks in the HXR emission flux. This flare supports the overall contraction picture of flares: a descending motion of the LT source, in addition to converging and unshearing motion of FPs. All results indicate that the magnetic field was very highly sheared before the onset of the flare.

Key words: Sun: activity — Sun: magnetic fields — Sun: flares

1 INTRODUCTION

In recent years, we have seen a kind of contracting motion in flare loops during the rising phase of many solar flares. Using X-ray observations made by the Ramaty High-Energy Solar Spectroscopic

* Supported by the National Natural Science Foundation of China.

Imager (*RHESSI*) (Lin et al. 2002), Sui & Holman (2003) firstly reported a descending motion of the loop-top (LT) source in the M-class flare on 2002 April 15. Following this result, many other events have been reported to show altitude decreases in the LT source, or even contracting motions of entire Ultraviolet/Extreme Ultraviolet (UV/EUV) flaring loops (Sui et al. 2004; Li & Gan 2005, 2006; Veronig et al. 2006; Joshi et al. 2009). This kind of phenomenon can still be well explained in the framework of common flare models. For example, the descending motion of the LT source was explained as the formation of a current sheet in the framework of the standard flare model based on the temperature structure between the LT source and the coronal source (Sui & Holman 2003). Some other models can also be used to explain the descending motion of the LT source, linking the shrinking of a cusp structure to a round shape (Forbes & Acton 1996) and collapsing magnetic trap (Veronig et al. 2006).

One obstacle to the above or similar explanations is the converging motion between flare conjugate kernels, which was found to occur simultaneously with the descending motion of the LT source (Ji et al. 2004, 2006, 2007; Zhou et al. 2008; Liu et al. 2009). The reported converging motion between flare kernels is a kind of unshearing motion and is regarded as a signature of energy released by magnetic reconnection in a sheared magnetic field or between highly sheared flux ropes (Ji et al. 2007, 2008). Joshi et al. (2009) reported a long duration ($\sim$ 11 min) contraction of flare loops for the M 7.6 flare on 2003 October 24. The contraction obviously includes a short term converging motion between hard X-ray (HXR) footpoints (FPs). They employed a 3D reconnection model (Somov et al. 2002) to explain this phenomenon. From this model, the converging motion between HXR FPs can be reproduced. Therefore, whether there is a correlation between the converging motion of HXR FPs or kernels and the descending motion of the LT source is a key factor to determine the physical mechanism of energy release in the rising phase of solar flares. For this kind of correlation, the detailed case studies in the literature are rather rare. The reason for this is that the LT source of disk events or FPs of limb events inevitably suffer from the projection effect. Furthermore, HXR FPs are often missing in the rising phase of flares due to insufficient photons in higher energy bands.

Using high-cadence observations of the Hα blue wing in an M-class flare taken from the Ganyu Solar Station, Ji et al. (2006) reported that the time profile of the rate of change of flare shear (unshearing rate) seems to be correlated with the peaks of HXR emissions. By analyzing the motion of UV kernels with high-quality 1600 Å images observed by the Transition Region and Coronal Explorer (*TRACE*) of a flare on 2002 July 26, Zhou & Ji (2009) reported that the peaks in the unshearing rate of the flare shear are correlated with *RHESSI* HXR emission peaks. This kind of correlation strongly suggests that free magnetic energy is released by magnetic reconnection inside sheared magnetic fields. For this kind of correlation, we also need more detailed case studies.

With the above motivations, we analyze the X 7.1 limb flare on 2005 January 20, focusing on the morphological evolution of X-ray sources. In Section 2 we give a short review of the published results for this flare and the related observations. We present the results in Section 3, and summarize the results in Section 4.

2 OBSERVATIONS

On 2005 January 20, a strong two-ribbon flare occurred in the active region NOAA 10720 (N12W58). The flare is classified as X 7.1 according to the *GOES* system, and is one of the most famous flares in solar cycle 23 because of its extremely strong impact in terms of terrestrial measurements. It caused unprecedented very hard high-energy proton enhancement that was near the Earth, including the second largest ground-level enhancement of cosmic ray intensity in observational history (Simnett 2006). The flare also showed pronounced gamma-ray emissions with a photon energy of up to 200 MeV (Hurford et al. 2006; Krucker et al. 2008). Many papers have appeared discussing this event, concentrating on the nature of high-energy particles produced by the flare. Detailed timing analysis showed that high energy protons were accelerated by the flare itself (Simnett 2006;

Grechnev et al. 2008). Grechnev et al. (2008) gave a comprehensive multi-wavelength analysis of this flare. Though still emphasizing the nature of energetic particles, they also reported that the magnetic elements of the active region producing this flare underwent a notable shearing motion along the neutral line. By giving a detailed multi-wavelength analysis with an emphasis on vector magnetograms taken by the Huairou Solar Observing Station, Wang et al. (2009) found unambiguous rapid enhancement of horizontal magnetic fields during the flare. They also reported the emergence of highly-sheared magnetic fields in the active region before the flare.

This event was detected by many spacecraft and ground-based solar observatories. The soft X-ray (SXR) fluxes of this flare were recorded by *GOES*.

Figure 1(a) shows the SXR fluxes at 0.5–4 and 1–8 Å. These fluxes show that this flare was a typical long duration event, lasting about 1 hour (06:30–07:30 UT). The flux of 0.5–4 Å gradually rose and reached a peak at 07:01 UT, followed by a long decreasing trend. This event was also well observed by *RHESSI* (Lin et al. 2002). Figure 1(b) shows the *RHESSI* lightcurves at different energy bands. The time resolution is 4 s, which corresponds to the spin period of the *RHESSI* spacecraft. The HXR lightcurves (≥ 25 keV) started rising from 06:39:00 UT, rapidly increased from 06:42:00 UT, and reached the main peak around 06:45:00 UT.

2.1 The Evolution of the LT Source and FPs

Using the *RHESSI* data, we make a series of maps at several energy bands to elucidate the detailed evolution of this flare. The maps were reconstructed with the CLEAN algorithm (Hurford et al. 2002) using front detector segments 3–8 with a natural weighting scheme.

Figure 2(a) shows an overall picture of this flare with HXR emissions at 10–15, 25–50, and 50–100 keV overlaid on a magnetogram observed by the Michelson Doppler Imager on board the Solar and Heliospheric Observatory (SOHO/MDI). The X-ray images were made at 06:40:00 UT. The magnetogram was taken at 06:03 UT, and was rotated to 06:40:00 UT. The dash-dotted line represents the simplified magnetic polarity inversion line (PIL). From Figure 2(a), we find that two compact HXR sources (25–50/50–100 keV) lie in the regions with an opposite magnetic polarity field, and are connected by an obvious X-ray loop (10–15 keV). The two HXR sources at higher energies are two conjugate FPs. In Figure 2(b), we overplot contours of X-ray emissions at energy bands of 25–50 and 50–100 keV and the contours of 1600 Å emissions on a whitelight image. Both 1600 Å and whitelight images were observed by the Transition Region and Coronal Explorer (TRACE). The 1600 Å images show that this event is a typical two-ribbon flare. From the whitelight images, we can see that the active region is composed of two main sunspots with some satellite spots. Compared with Figure 2(a), we find that the southern/northern sunspot has positive/negative polarity. The HXR FPs are located on the edge of an umbra associated with the main sunspots, and are situated over the outer edge of two bright 1600 Å ribbons (Krucker et al. 2008).

The flare at different energy bands exhibits different spatial structures and evolutionary patterns (Fig. 3). The flare at 10–15 keV shows an obvious loop structure with a bright round tip, which can be regarded as an LT source. The flare loop is asymmetric: the northern leg is apparently shorter than the southern one. The legs slowly disappear in an upward direction while the LT source remains compact and bright. The LT source has a noticeable motion toward lower altitudes during the rising phase, and then moves upward. The main feature of *RHESSI* images at 50–100 keV is represented by two well-defined FPs. The first footpoint appears in a negative magnetic field at ∼06:39:48 UT, and another footpoint develops in a positive magnetic field 10 s later. The sequence of activity is described as follows. The northern footpoint (NFP) moved to the east, with its trajectory of motion roughly parallel to the PIL. The southern footpoint (SFP) simultaneously showed movement from the southeast to the northwest. At 06:56 UT, another weaker footpoint appeared to the east of the NFP, lasting for 3 min, and then quickly disappeared (Fig. 3(k)). From 07:00 UT, the NFP had an obvious separating motion to the northeast in the direction roughly perpendicular to the magnetic

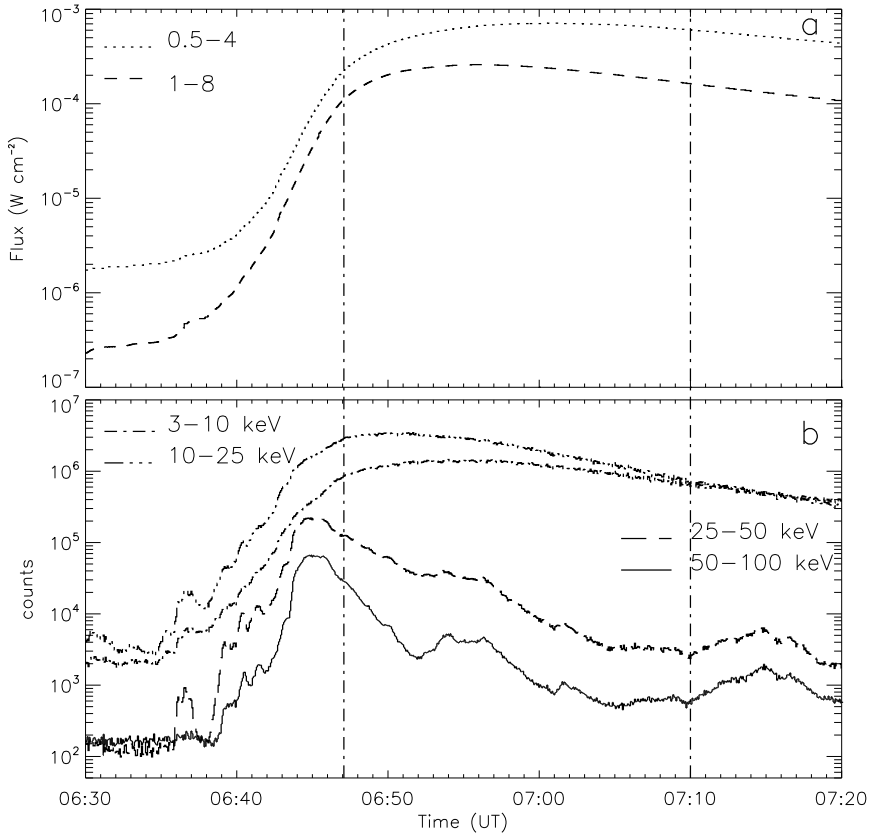

Fig. 1 *GOES* and *RHESSI* light curves. (a) *GOES* 0.5–4 and 1–8 Å fluxes. (b) *RHESSI* light curves obtained in four energy bands with 4 s integration: 3–10 (*dash-dotted*), 10–25 (*dash-dot-dotted*), 25–50 (*dashed*) and 50–100 keV (*solid*). The vertical dot-dashed lines mark the time range for the missing HXR FPs.

PIL, while the SFP had a slight separating motion. The main features at 25–50 keV were quite similar to those at 50–100 keV reported above. According to Figure 3, from ∼06:40:06 UT, two distinct FPs at 25–50 keV appeared at the same positions as those at 50–100 keV. Moreover, another bright source could be observed at the top of the flare loop, which only remained for about 1 min then quickly disappeared (Fig. 3(b)). After 6 min, this source gradually re-appeared at the same position (Fig. 3(f)). Meanwhile, the FPs moved toward this source and gradually became weaker. Finally, this source mixed with FPs, and developed into the loop. The loop with the bright top source lasted 20 min then gradually disappeared. From 07:10 UT, two distinct FPs appeared, and their positions and motions were similar to those at 50–100 keV. According to Figure 5(a), the HXR emission light curve has a peak during the interval from 07:10 to 07:20 UT. This peak of HXR emission indicates the tide of magnetic reconnection. We, therefore, believe that the re-appearance of the FPs is associated with this peak. The FPs can also be found in the images at 15–25 keV, but only during the last $\sim$ 1 min.

In general, the lower X-ray energy emission dominates the flare loop while higher X-ray energy emission appears as FPs. It is very rare to observe an HXR loop (Liu et al. 2006; Ning & Cao 2010).

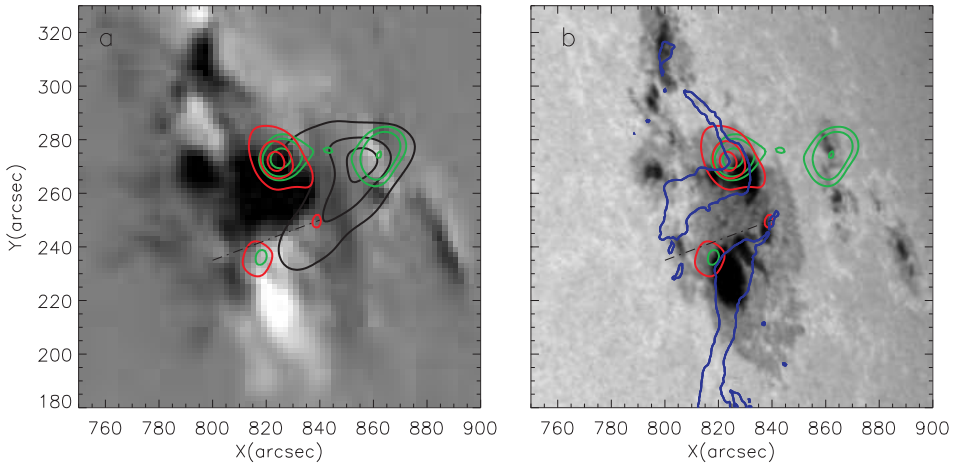

Fig. 2 An overall picture of the flare in multiple wavelengths. (a) The contours of X-ray emission at 10–15 (*black*, 06:40:00–06:40:12 UT), 25–50 (*yellow*, 06:40:00–06:40:20 UT), and 50–100 keV (*red*, 06:40:00–06:40:30 UT) overlaid on the MDI line-of-sight magnetogram (06:03:00 UT). (b) Contours of TRACE UV 1600 Å (*blue*) emission and *RHESSI* X-ray emissions (25–50 (*yellow*) and 50–100 keV (*red*)) overlaid on the TRACE whitelight image. All images are rotated to 06:40:00 UT.

We assume that this phenomenon is caused by unusually strong chromospheric evaporation. Liu et al. (2006) found a flare showing HXR emission from the flare loop, and noticed a movement in the centroids of the HXR sources from FPs to the LT source. They regarded this phenomenon as evidence of chromospheric evaporation. Jin & Ding (2008) analyzed the flare described in this paper and found that the density of the loop legs increased. They verified the existence of chromospheric evaporation.

2.2 Relationship between the LT Source and FPs

The main point of this study focuses on the relationship between the motion of the LT source and the FPs. We use the centroid of the LT source and FPs to analyze the motions in detail. For the LT source, we select a region, in which the top of the flare LT can be entirely included during the whole flare process. We use emission of all pixels above 80% of the peak flux in the selected region to get the centroid of the LT source. For computing the centroids of FPs, we only choose the images that have two distinct FPs and select two boxes which can encompass FPs. The centroids of HXR FPs are also computed using the emissions of all pixels above 80% of the peak value in the selected regions.

We overlay the centroids of the LT sources (10–15 keV) and the FPs (50–100 keV) on a SOHO/MDI line-of-sight magnetogram in Figure 4. The color representing time is used to indicate the trajectories of the LT source and FPs. From Figure 4, the motion of the LT source shows a clear early descending and later ascending motion. The FPs show a converging motion along the magnetic PIL firstly in the antiparallel direction, and then separated from each other. According to the kinematics of the LT source and FPs, we can divide the flare process into two main phases. The cutting point is around 06:45 UT, corresponding the maximum phase of the flare. The first phase, from 06:30 to 06:45 UT, is called the contraction phase, and is marked by the downward motion of the LT source and converging motion of the FPs. After 06:45 UT, the motions of the LT source and the FPs are the same as the prediction of the classical flare model. This phase can be called the expansion phase.

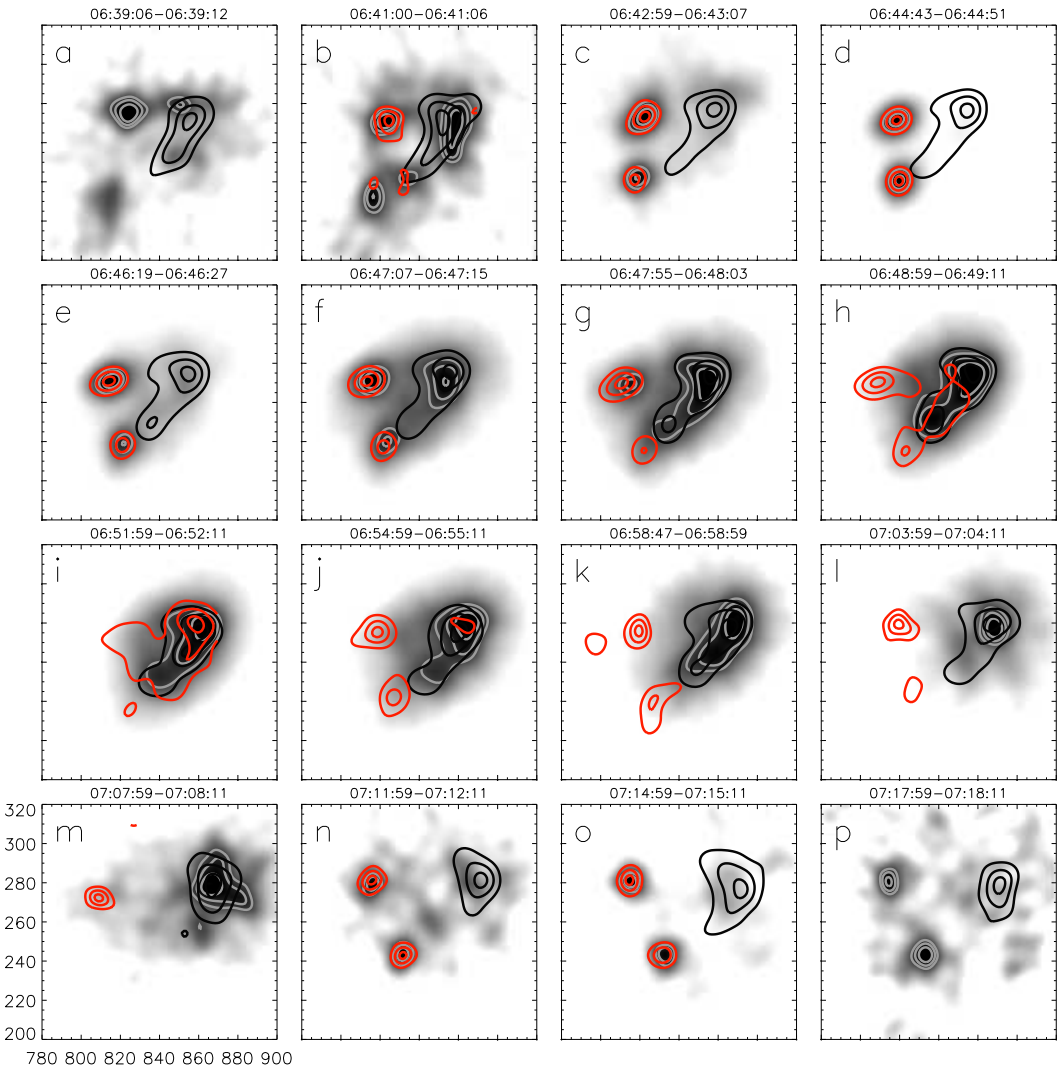

Fig. 3 Sequence of images from *RHESSI* at 10–15 keV (*black* contours) and 50–100 keV (*red* contours) are overlaid images at 25–50 keV (*gray* contours). For the 10–15 keV images, the contour levels are at 60%, 80%, and 90% of each image's peak flux. For the 25–50 and 50–100 keV images, the contour levels are 70%, 80%, and 90%, respectively.

The projected position of the LT source can still be used to express the height of the flare loop (Sui & Holman 2003). Here, the altitude is defined as the distance along the main axis of the motion of the LT, between the centroid of the LT source and the center of a line connecting two conjugate FPs at 06:45:10 UT at 50–100 keV (Veronig et al. 2006; Joshi et al. 2009). The main axis of motion for the LT source is determined by fitting a line to the centroids of LT sources (Veronig et al. 2006). In our case, the main axis is offset from the radial direction by 23.2 degrees toward the west (Fig. 4). Because this flare occurred at the west limb, the positions of magnetic PIL and HXR FPs are seriously affected by the projection effect. We have to transform their positions as if the flare were observed at the center of the solar disk.

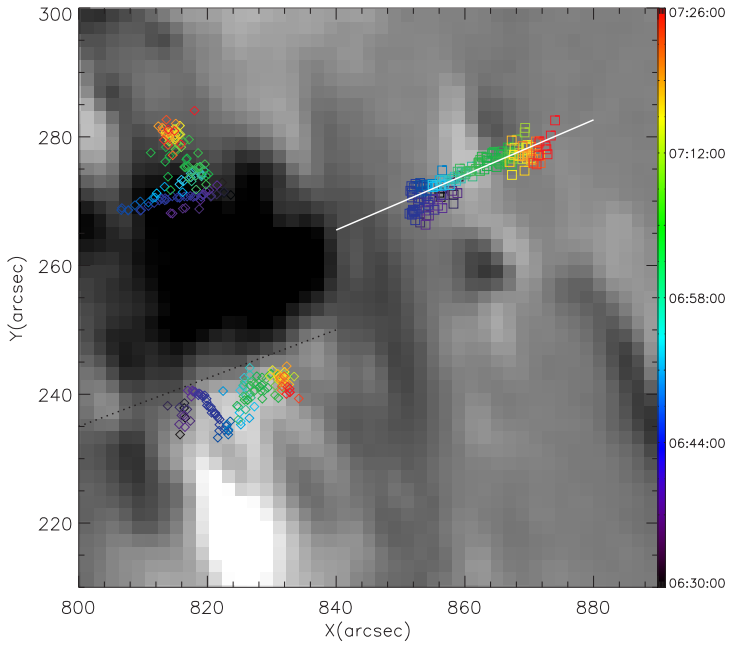

Fig. 4 Centroids of the *RHESSI* LT sources at 10–15 keV and the FPs at 50–100 keV are overlaid on an MDI longitudinal magnetogram (*black*: negative polarity, *white*: positive polarity). The evolution of HXR images is from 06:30 to 07:26 UT. The MDI image, taken at 06:03:30 UT, was rotated to 06:50 UT. The white line is the fitting line to the centroids of LT sources.

The time profiles for the altitudes at three energy bands are plotted in Figure 5(b). For comparison, the corrected HXR time profiles at different energy bands are plotted in Figure 5(a). We find that in the rising phase of the flare, the LT sources observed at 6–10, 10–15 and 15–20 keV energy bands are almost co-spatial (or spatially mixed) and descend with similar speed, ranging from 5.38 km s^{-1} (6–10 keV) to 6.76 km s^{-1} (15–20 keV). Meanwhile, the time profile of the distance between the two FPs at 25–50 keV, after correcting for the effect of projection, is plotted in Figure 5(c). It clearly shows that the contraction of flare loops consists of the descending motion of the LT source and the converging motion of the two conjugate FPs.

It is worth noting that the spatial evolution of the LT source is rather complex from 06:40 UT to the expansion period: the height of flare loops undergoes a second decrease, starting at about 06:43:00 UT. The second contraction can be seen from Figure 5(b)–(c) (see the vertical dotted line). It is worth noting that the second contraction starts with the rising time of the gamma ray emission of the flare (> 300 keV, Fig. 6(a)).

During the contraction phase, X-ray sources are all mixed together, which confirms the earlier findings by Shen et al. (2008). They explained this as the signature of reconnection between sheared flux ropes. During the expansion period, the temperature structure of the flare loops shows a well ordered distribution, i.e., a higher temperature source is located above a lower temperature source (Fig. 5(b)). This result also confirms earlier works by Liu et al. (2009) and Shen et al. (2008), and it is in agreement with what the standard flare model predicts: the site where energy release occurs is above the flare loop. We also find that the flare loop at a higher energy band moves upward faster (14.5 km s^{-1} at 15–20 keV) than that at the lower energy band (8.16 km s^{-1} at 6–10 keV) during the expansion period. Moreover, the ascending motion of the source of the LT in the flare as observed in

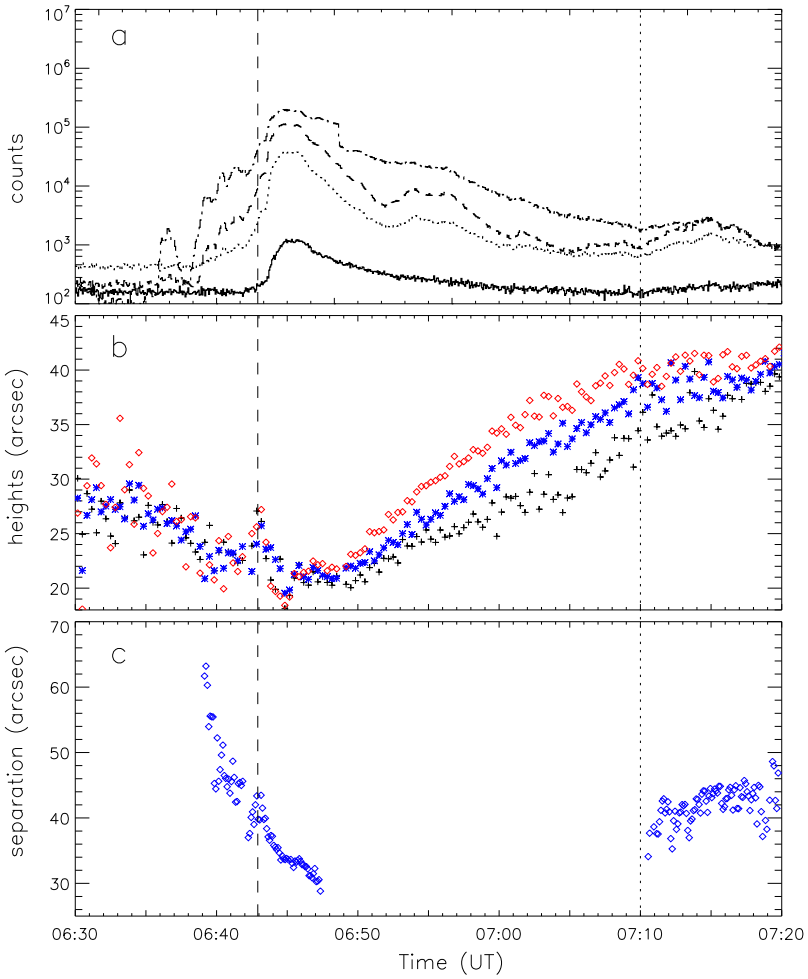

Fig. 5 (a) *RHESSI* HXR light curves obtained in four energy bands with 4s integration: 25–50 (*dash-dotted*), 50–100 (*dashed*), 100–300 (*dotted*) and 300–500 keV (*solid*). (b) Evolution of the height of the LT source as obtained at 6–10 keV (*black pluses*), 10–15 keV (*blue stars*) and 15–20 keV (*red diamonds*). (c) The separation of the FP sources in 25–50 keV. The dashed line marks the starting time of the second contraction process. The dotted line marks the starting time of the re-appearance of HXR FPs.

higher energy bands (> 10 keV) has an obvious deceleration. The deceleration starts with the rising of HXR emission at 07:10 UT, corresponding to the starting time of the third period in Figure 1. The reduced ascending speed has shortened the obvious height separation among the LT sources at different energies. This phenomenon is in agreement with the findings made by Liu et al. (2006).

2.3 Flare Shear

The spatial evolution of FPs can provide additional information about magnetic reconnection. According to the definition of Ji et al. (2007), the flare shear can be used to measure the shear extent of the reconnected magnetic loops. We measure the flare shear using the FPs at 25–50 and

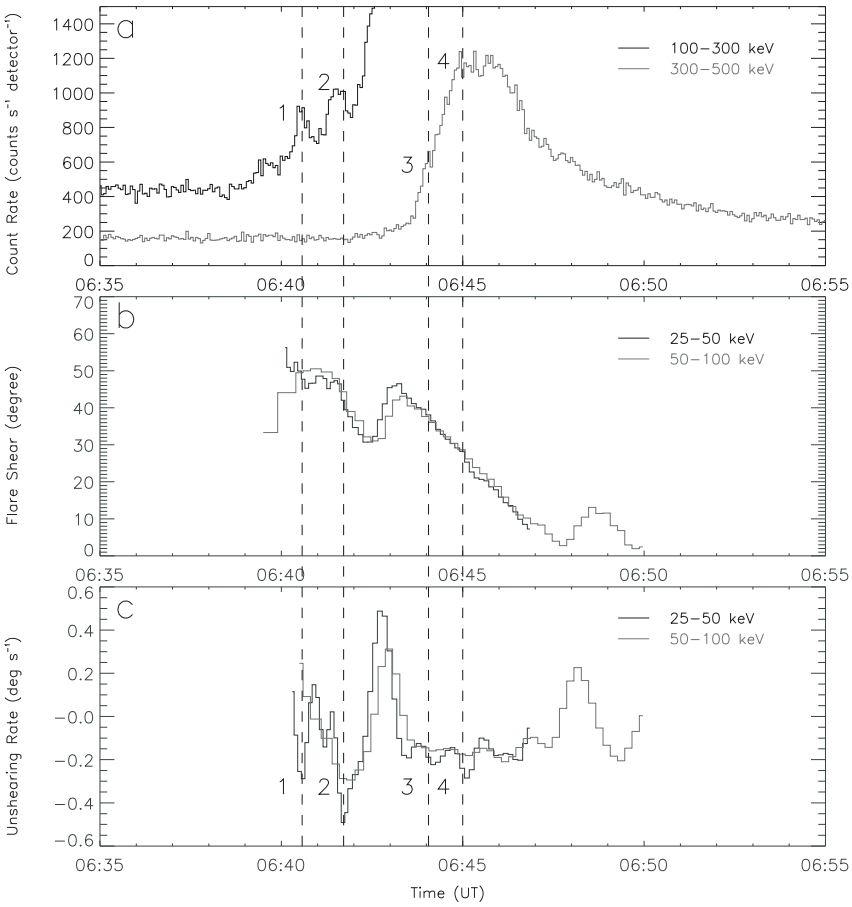

Fig. 6 (a) Time profiles of *RHESSI* X-ray light curves obtained at 100–300 (*black*) and 300–500 keV (*gray*). (b) Time profiles of the flare shear obtained at 25–50 (*black*) and 50–100 keV (*gray*). (c) The unshearing rate at 25–50 (*black*) and 50–100 keV (*gray*).

50–100 keV after correcting for the effect of projection (Fig. 6(b)). Both of the time profiles describing the flare shear are similar and rapidly fluctuate, and show a decrease during the rising phase. Su et al. (2007) presented a statistical investigation of the shear motion of the UV/EUV FPs, and found that 86% (43 out of 50) of flares show a strong-to-weak shear change. Ji et al. (2006) explained the decrease of flare shear as the result of reconnection between strongly sheared magnetic fields. Checking Figure 6(b), we find that the initial flare shear, after being corrected for projection, is nearly 50 degrees. The higher initial flare shear indicates a strongly sheared magnetic field before the onset of this flare. For this active region (NOAA 10720), Grechnev et al. (2008) and Wang et al. (2009) reported a significant shear motion of sunspots or the emergence of sheared sunspots with opposite polarities before the flare. This shear motion can create the strongly sheared magnetic field.

The variation of flare shear can reflect the kinematic process of magnetic energy release in the corona (Ji et al. 2007). The peak in the unshearing rate can be assumed to be the signature of a rapid release of free magnetic energy. A linear fitting with five points gives the unshearing rate of that point. The time profiles of the unshearing rate at two kinds of energy bands during the contraction phase are plotted in Figure 6(c). Compared with Figure 6(a), we note that four peaks in

the unshearing rate were correlated with HXR emission peaks (100–300 and 300–500 keV). These results confirm an earlier work by Zhou & Ji (2009), who reported that the peaks of HXR emission were well correlated with the peaks of the unshearing rate.

3 SUMMARY

Since Sui et al. (2003) found that the height of the flare loop decreased during the rising phase, the contracting motion of the flare loop has attracted more and more attention in solar physics. The contracting motion is mainly composed of two aspects: the downward motion of the LT source and the converging motion between FPs. The apparent downward motion of the X-ray LT source or contraction of UV/EUV flare loops has been studied in detail by many authors (Sui & Holman 2003; Sui et al. 2004; Li & Gan 2005, 2006; Veronig et al. 2006; Ji et al. 2006; Shen et al. 2008; Zhou & Ji (2009); Joshi et al. 2009). The converging motions of Hα kernels or HXR FPs are also reported in some flare events (Ji et al. 2004, 2006; Zhou et al. 2008). However, it is hard to simultaneously observe the downward motion of the LT source and the converging motion between FPs, because the HXR FPs are often missing in the rising phase due to insufficient photons in higher energy bands. In this paper, we give a detailed analysis of the X 7.1 flare on 2005 January 20. This flare is a rare strong event, showing a clear loop with a bright LT source, and two distinct HXR FPs. Especially in the rising phase, the HXR FPs could be well observed and lasted for 6 min. Therefore, this flare gives us a good opportunity to investigate the relationship between the motions of the LT source and the FPs in the rising phase. We also get the flare shear and compare the unshearing rate with the higher HXR emission. Our results can be summarized as follows:

(1) There is a temporal correlation between the time profiles of altitude in the LT source and that of the distance between FPs. During the rising phase, the downward motion of the LT source corresponds to the converging motion of the FPs. We confirm that this phenomenon reflects the overall contracting picture of a flare loop during X-ray emission.
(2) The temperature distribution of flare loops along the path of contraction is very irregular, showing no spatial order at all. A normal temperature distribution only exists along the path of expansion. This result confirms the earlier findings by Shen et al. (2008) and Liu et al. (2009).
(3) Our results show that the motion of FPs, after being corrected for projection, is the same as the prediction of the rainbow reconnection model (Somov 1986). Firstly, the FPs move toward each other along the magnetic PIL, reducing the distance between them. The motions of FPs in an antiparallel direction during the rising phase are common (Bogachev et al. 2005; Yang et al. 2009). At about 06:45 UT, the FPs passed through a "critical point" (Somov et al. 2005), and then the northern footpoint source departed from the magnetic PIL and the southern FP source almost remained steady.
(4) The value of flare shear has a rapidly fluctuating decrease, changing from 50 to 10 degrees. The decrease of flare shear has been reported in many two-ribbon flares (Bogachev et al. 2005; Ji et al. 2006; Zhou et al. 2008; Zhou & Ji 2009; Yang et al. 2009). We further find that four peaks in the unshearing rate temporally correlate with peaks in HXR ($\geq$ 100 keV) emission. This confirms our earlier work about an M 1.0 class flare (Zhou & Ji 2009).

According to the above results, we suggest that the contraction of the flare loop occurs during the rising phase and is composed of three aspects: the downward motion of the LT source, the converging motion of FPs along the magnetic PIL and the decrease of flare shear. Ji et al. (2007) gave a force-free sheared magnetic model to explain the converging motion in HXR FPs and the decrease in flare shear. They believed that the magnetic reconnection would reduce the shear extent of the flare arcades, and the less-sheared arcades would have a smaller height and span. This height indicates the altitude of the LT source, and span can be considered as the distance between the HXR FPs. Since it is very rare to observe the HXR FPs in the rising phase of the flare, more observations

with high temporal and spatial resolution are needed to study the unshearing contraction of flare loops.

Acknowledgements The authors thank the *RHESSI* and TRACE teams for providing data and software. We thank an anonymous referee for helpful comments and valuable suggestions, and the editor for improving the English. This work is supported by the National Natural Science Foundation of China (Grant Nos. 10833007, 11173062, 10921303, 11178002, 10928307 and 11111120071) and the National Basic Research Program of China (973 program, Grant No. 2011CB811402). VM is supported by the Chinese Academy of Sciences via a visiting professorship for senior international scientists with grant No.2010t2j36 and by the joint RFBR-CNSF (Grant No.11-02-91175). The work of Zhou is supported by the Open Research Program of the Key Laboratory of Solar Activity of National Astronomical Observatories, and the Scientific Research Foundation of Nanjing University of Information Science and Technology (Grant Nos. S8110136001 and N1081005072).

References

Bogachev, S. A., Somov, B. V., Kosugi, T., & Sakao, T. 2005, ApJ, 630, 561
Forbes, T. G., & Acton, L. W. 1996, ApJ, 459, 330
Grechnev, V. V., Kurt, V. G., Chertok, I. M., et al. 2008, Sol. Phys., 252, 149
Hurford, G. J., Schmahl, E. J., Schwartz, R. A., et al. 2002, Sol. Phys., 210, 61
Hurford, G. J., Krucker, S., Lin, R. P., et al. 2006, in Bulletin of the American Astronomical Society, 38, AAS/Solar Physics Division Meeting #37, 255
Ji, H., Wang, H., Goode, P. R., Jiang, Y., & Yurchyshyn, V. 2004, ApJ, 607, L55
Ji, H., Huang, G., Wang, H., et al. 2006, ApJ, 636, L173
Ji, H., Huang, G., & Wang, H. 2007, ApJ, 660, 893
Ji, H., Wang, H., Liu, C., & Dennis, B. R. 2008, ApJ, 680, 734
Jin, M., & Ding, M. 2008, PASJ, 60, 835
Joshi, B., Veronig, A., Cho, K.-S., et al. 2009, ApJ, 706, 1438
Krucker, S., Hurford, G. J., MacKinnon, A. L., Shih, A. Y., & Lin, R. P. 2008, ApJ, 678, L63
Li, Y. P., & Gan, W. Q. 2005, ApJ, 629, L137
Li, Y. P., & Gan, W. Q. 2006, ApJ, 644, L97
Lin, R. P., Dennis, B. R., Hurford, G. J., et al. 2002, Sol. Phys., 210, 3
Liu, W., Liu, S., Jiang, Y. W., & Petrosian, V. 2006, ApJ, 649, 1124
Liu, W., Petrosian, V., Dennis, B. R., & Holman, G. D. 2009, ApJ, 693, 847
Ning, Z. J., & Cao, W. D. 2010, ApJ, 717, 1232
Shen, J., Zhou, T., Ji, H., et al. 2008, ApJ, 686, L37
Simnett, G. M. 2006, A&A, 445, 715
Somov, B. V. 1986, A&A, 163, 210
Somov, B. V., Kosugi, T., Hudson, H. S., Sakao, T., & Masuda, S. 2002, ApJ, 579, 863
Somov, B. V., Kosugi, T., Bogachev, S. A., Sakao, T., & Masuda, S. 2005, Advances in Space Research, 35, 1700
Su, Y., Golub, L., & Van Ballegooijen, A. A. 2007, ApJ, 655, 606
Sui, L., & Holman, G. D. 2003, ApJ, 596, L251
Sui, L., Holman, G. D., & Dennis, B. R. 2004, ApJ, 612, 546
Veronig, A. M., Karlický, M., Vršnak, B., et al. 2006, A&A, 446, 675
Wang, J., Zhao, M., & Zhou, G. 2009, ApJ, 690, 862
Yang, Y.-H., Cheng, C. Z., Krucker, S., Lin, R. P., & Ip, W. H. 2009, ApJ, 693, 132
Zhou, T., Ji, H., & Huang, G. 2008, Advances in Space Research, 41, 1195
Zhou, T.-H., & Ji, H.-S. 2009, RAA (Research in Astronomy and Astrophysics), 9, 323